

EFFECTS OF CHANGING SURFACE HEAT FLUX ON THE ATMOSPHERIC BOUNDARY LAYER FLOW OVER FLAT TERRAIN

ANTONY Z. OWINOH (owinoh@pik-potsdam.de)

Potsdam Institute for Climate Impact Research, Potsdam, Germany

JULIAN C. R. HUNT (jcrh@cpom.ucl.ac.uk)

Centre for Polar Observation and Modelling, University College London, UK &

JM Burger Centre, Delft University of Technology, The Netherlands

ANDREW ORR (ao@cpom.ucl.ac.uk)

Centre for Polar Observation and Modelling, University College London, UK

PETER CLARK (peter.clark@metoffice.com)

Joint Centre for Mesoscale Meteorology (JCMM), Reading, UK

RUPERT KLEIN (rupert.klein@zib.de)

Potsdam Institute for Climate Impact Research, Potsdam, Germany & FB

Mathematik and Informatik, Free University Berlin, Germany

H. J. S. FERNANDO (j.fernando@asu.edu)

*Environmental Fluid Dynamics Program, Department of Mechanical and Aerospace
Engineering, Arizona State University, Tempe, USA*

FRANS T. M. NIEUWSTADT (f.nieuwstadt@wbmt.tudelft.nl)

JM Burger Centre, Delft University of Technology, The Netherlands

Abstract. We examine the unsteady response of a neutral atmospheric boundary layer (ABL) of depth h and friction velocity u_* when a uniform surface heat flux is applied abruptly or decreased rapidly over a time-scale t_θ less than about $h/(10u_*)$. Standard Monin-Obukhov (MO) relationships are used for the perturbed eddy viscosity profile in terms of the changes to the heat flux and mean shear. Analytical solutions for changes in temperature, mean wind and shear stress profile are obtained for the surface layer, when there are small changes in $h/|L_{MO}|$ over the time-scale $t_{MO} \sim |L_{MO}|/(10u_*)$ (where L_{MO} and t_{MO} are the length and time-scales respectively). They show that a maximum in the wind speed profile occurs at the top of the thermal boundary layer for weak surface cooling, i.e. a wind jet, whereas there is a flattening of the profile and no marked maximum for weak surface heating. The modelled profiles are approximately the same as those obtained from the UK Met Office Unified Model when operating as a mesoscale model at 12 km horizontal resolution. The theoretical model is modified when strong surface heating is suddenly applied, resulting in a large change in $h/|L_{MO}|$ ($\gg 1$), over the time-scale t_{MO} . The eddy structure is predicted to change significantly and the addition of convective turbulence increases the shear turbulence at the ground. A low level wind jet can form, with convective turbulence adding to the mean momentum of the flow. This was verified by our laboratory experiment and direct numerical simulations. Additionally, it is shown that the effects of Coriolis acceleration diminish (rather than as suggested in the literature, amplify) the formation of the wind jets in the



© 2004 Kluwer Academic Publishers. Printed in the Netherlands.

situations considered here. Hence only when the surface heat flux changes over time-scales greater than $1/f$ (where f is the Coriolis parameter) does the ABL adjust monotonically between its equilibrium states. These results are also applicable to the ABL passing over spatially varying surface heat fluxes.

Keywords: Atmospheric boundary layer modelling, Convection, Surface heat flux, Surface layer, Wind jets

1. Introduction

Following the discovery by Richardson (1923) of how heat flux variations can significantly affect the turbulence, Monin and Obukhov (1954) showed how this leads to universal profiles for the mean velocity and temperature over terrain with very low slopes. Garratt (1992) reviews the effects of spatial and temporal variations of surface heat flux over flat terrain. The conceptual understanding, analytical theories, and computational modelling of characteristic profiles of temperature, velocity etc, are well developed. Note that they all increase or decrease monotonically from the ground to the top of the boundary layer. Businger played a crucial role in these scientific advances and in ensuring the reliability of the data (e.g. Businger *et al.*, 1971).

In non-equilibrium conditions when the variations occur on space and time-scales comparable with or less than those for the natural development of the boundary layer (i.e. 1–10 km or 10^3 – 10^4 s), new physical effects occur which have only partly been observed and studied; also models differ in their prediction, especially because of differences in how they calculate changes in Reynolds stress (or eddy viscosity). These changes occur daily when neutral or convective boundary layers become stably stratified when passing over a cold surface (e.g. in the evening or due to sudden cloud formation shielding sunlight), or when stable or neutral boundary layers become convectively unstable over heated surfaces (e.g. at dawn, sea-land transition or due to sudden cloud dissolution), then the changes to the stability affect the turbulence structure and the mean shear stresses (Garratt, 1992).

The most difficult features to predict correctly in these complex flows are the profiles of mean velocity and turbulence, notably the formation of low level wind jets. Richardson (1923) found between low hills (~ 100 m) at Benson that the maximum wind velocity can be 70% greater than the geostrophic wind. Thorpe and Guymer (1977) observed ‘nocturnal’ jets occurring at dawn over Southern England at a height 200–400 m with the wind maximum 50% greater than the ageostrophic wind. Over the Great Plains (Bonner, 1968) the formation of the jets was explained, following Blackadar (1957), in terms of the

time variations of heat flux and Coriolis effects. A similar explanation is usually given for low level wind jets over the land-sea transition in terms of spatial variation in heat flux and Coriolis effects (Smedman et al., 1995). Low level jets in convective conditions have also been observed in rapidly changing flows over the Baltic (Smedman; personal communication). The second notable type of flow profile distortion is the unsteady transition front, such as strong gravity current fronts in land-sea breezes moving over a wide area (Simpson, 1994). Clearly to understand these common types of distorted boundary layer flow it is necessary to study the relative importance of the varying surface heat flux (typically over a time less than 10^4 s or a length scale of 1–10 km), significant elevation change (e.g. where slopes are of the order 10^{-3}) and Coriolis forces (on a time-scale of order $1/f$, where f is the Coriolis parameter).

In this paper we focus on flat terrain and the effects of turbulent structure on the profiles, especially near the surface where Coriolis effects are weak. In a subsequent paper we will use similar analysis and numerical simulations to study the effect of the changing boundary layer over small slopes, which previous authors (e.g. Scorer, 1954; Hunt et al., 2003a) have shown are significant.

Extending the calculation of Townsend (1965) for the temperature perturbation when the surface heat flux over a flat surface is changed at time $t=0$, we first develop a simple parameterized model for the effect of buoyancy on turbulence when a weak heat flux is applied abruptly over a flat surface. By calculating how the turbulent shear stresses are modified by weak changes in stability, following the Richardson-Monin-Obukhov scaling (Turner, 1973), the mean velocity profiles are calculated. We extend the analysis to consider the effects of strong heat flux when the turbulence structure changes. Using a model of eddy viscosity in strong thermal convection (Wyngaard and Brost, 1984) the mean profiles are presented and the significance of Coriolis forces investigated.

In most global circulation models (GCM) used in numerical weather prediction (NWP), the boundary layer profiles are not calculated explicitly but are assumed to have quasi-steady form (i.e. monotonically increasing from the ground). In mesoscale NWP models, profiles are calculated using an eddy viscosity approximation for the shear stress. Whereas these models are calibrated against data and perturbation models for flow over terrain and in quasi-steady conditions, they have not been tested in detail when the surface heat flux is applied abruptly or decreased rapidly. Therefore one of the aims of this paper is to compare mesoscale NWP profiles under these conditions with the equivalent profiles from the theoretical model. Additionally, understanding the

profiles may lead to improved boundary layer models for the GCMs and, for example, the correct forecasting of critical unsteady situations such as the evening transition.

The plan of the paper is as follows. The simple parameterised model is formulated in Section 2 and the solutions and results for weak and strong fluxes are presented in Section 3. Section 4 presents a comparison with numerical mesoscale modelling results and Section 5 is a brief presentation of a laboratory experiment and direct numerical simulations (DNS) results for strong convection applied to a shear flow. The paper concludes in Section 6 with a discussion.

2. Formulation of the Problem

2.1. EQUATIONS AND APPROXIMATE MODELS FOR WEAK TURBULENT FLUXES

We consider a 2-D steady uniform flow ($\partial/\partial t = 0$, where t is time) with mean velocity profile $U_B(z)$ and mean temperature $\Theta_B(z)$ (z is the vertical co-ordinate) being perturbed by its passage over a heated or cooled surface (see Figure 1). Thus the flow variables can be expressed as the sum of the perturbation and the background state of the boundary layer denoted by the subscript B , e.g. velocity $U = U_B(z) + u(x, z, t)$, potential temperature $\Theta = \Theta_B(z) + \theta(x, z, t)$. In general the perturbations vary with distance x (parallel to the wind). The linearised equations that describe the potential temperature perturbation θ is given by

$$\frac{\partial \theta}{\partial t} + U_B \frac{\partial \theta}{\partial x} + w \frac{\partial \Theta_B}{\partial z} = -\frac{\partial F_\theta}{\partial z}, \quad (1)$$

and u and w , the velocity perturbations in the x and z directions, respectively, satisfy

$$\frac{\partial u}{\partial t} + U_B \frac{\partial u}{\partial x} + w \frac{\partial U_B}{\partial z} = -\frac{\partial p}{\partial x} + \frac{\partial \tau_{xz}}{\partial z}, \quad (2a)$$

$$\frac{\partial w}{\partial t} + U_B \frac{\partial w}{\partial x} = -\frac{\partial p}{\partial z} + \frac{\partial \tau_{zz}}{\partial z}, \quad (2b)$$

$$\frac{\partial u}{\partial x} + \frac{\partial w}{\partial z} = 0. \quad (2c)$$

Here τ_{xz} and τ_{zz} are the perturbation shear stress and normal stress relative to τ_{Bxz} and τ_{Bzz} , respectively, for the undisturbed flow. Similarly F_θ is the perturbation heat flux relative to F_{θ_B} and p is the perturbation pressure relative to p_B . Note the streamwise derivative of stresses are negligible.

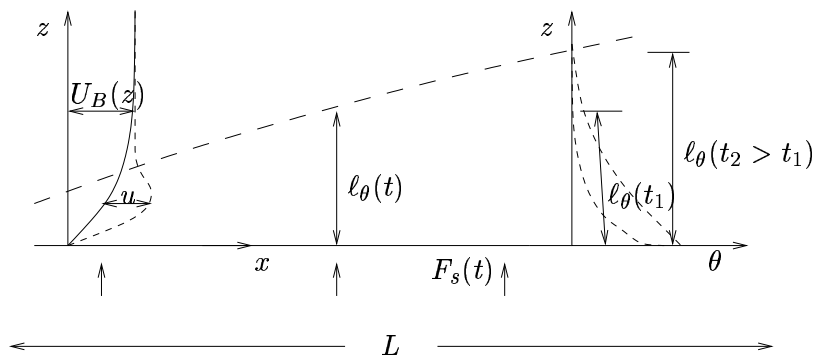


Figure 1. Schematic diagram for the thermal internal boundary layer for flow over a heated or cooled surface that varies in time over a time-scale t_θ , and horizontally over a very large length scale L . The perturbation velocity u , the perturbation potential temperature θ , and the thermal layer thickness $\ell_\theta(t)$, depend on the magnitude of the surface heat flux $F_s(t)$ and the background velocity profile $U_B(z)$.

2.2. SIMPLIFYING THE EQUATIONS AND ANALYSIS OF THE PERTURBED LAYERS

As usual in a scaling analysis, the relative magnitudes of each terms in the equations are determined by comparing with the advective term. We first need to consider the length scales in relation to the magnitude of u and w by considering (2c). Within the boundary layer, the vertical length scale over which the turbulence and mean velocity are perturbed is ℓ_θ , the thermal layer depth. The continuity equation implies that

$$\frac{u}{L} \sim \frac{w}{\ell_\theta} \Rightarrow w \sim \frac{\ell_\theta}{L} u.$$

where L is the horizontal length scale, assumed to be very long in the situation considered here. Since the flow is unsteady as a result of surface heating changing rapidly over a time scale $t_\theta (\ll L/U_B)$, the unsteady inertial term $\partial u / \partial t \sim u/t_\theta \gg uU_B/L$. However the spatial inertial terms $U_B \partial u / \partial x (\sim uU_B/L)$ and $w \partial U_B / \partial z (\sim uu_*/L)$, where u_* is the frictional velocity) can be neglected in (2a) when compared to $\partial u / \partial t$. Thence the perturbation pressure gradients are negligible compared to the unsteady inertial terms.

Based on these scale analyses and neglecting $\partial / \partial x$ (which can be verified *a posteriori* using the solution) the governing equations (1) and (2a) reduce to

$$\frac{\partial \theta}{\partial t} = -\frac{\partial F_\theta}{\partial z}, \quad (3)$$

and

$$\frac{\partial u}{\partial t} = \frac{\partial \tau}{\partial z}, \quad (4)$$

where $\tau = \tau_{xz}$ (i.e. we omit the subscript xz in the perturbation shear stress hereafter).

Equations for τ and the perturbation heat flux F_θ , in quasi-steady boundary layers where the turbulence is close to equilibrium, are derived using the gradient flux relation for the surface layer. This leads to relationships between the perturbations of velocity gradient, shear stress, heat flux, and temperature, in terms of the perturbation eddy viscosity $\Delta\nu_e$ and the perturbation diffusivity ΔK_e ; $\nu_e = \nu_B + \Delta\nu_e$ and $K_e = K_B + \Delta K_e$. Since $\tau_B + \tau = (\nu_B + \Delta\nu_e)\partial(U_B + u)/\partial z$, to first order

$$\tau = \Delta\nu_e \frac{\partial U_B}{\partial z} + \nu_B \frac{\partial u}{\partial z}, \quad (5a)$$

and similarly

$$F_\theta = -\Delta K_e \frac{\partial \Theta_B}{\partial z} - K_B \frac{\partial \theta}{\partial z}. \quad (5b)$$

For a boundary layer with initial constant temperature, $\partial\Theta_B/\partial z = 0$. Hence (5b) reduces to

$$F_\theta = -K_B \frac{\partial \theta}{\partial z}. \quad (5c)$$

We use the general relation between eddy viscosity and Richardson number, Ri , for weakly stratified shear flow (e.g. Turner, 1973) of $\nu_e = (1 - \hat{\alpha} Ri) \nu_e(Ri = 0)$, where $\hat{\alpha}$ is a coefficient that depends on the type of shear flow (see below). The eddy viscosity background state and its perturbation in a neutral surface layer ($Ri = 0$) are given by $\nu_B = \kappa u_* z$ and $\Delta\nu_e(Ri = 0) = (\nu_B \partial u / \partial z) / (\partial U_B / \partial z)$, where κ is the von Karman constant. Thence for $Ri \neq 0$, $\Delta\nu_e = \kappa u_* z ((\partial u / \partial z) / (\partial U_B / \partial z) - \hat{\alpha} Ri)$ and $Ri = (g/\theta_0)(\partial\theta/\partial z) / (\partial U / \partial z)^2$ (where g is the acceleration due to gravity and θ_0 is a reference potential temperature). To first order $Ri = ((g/\theta_0)\partial\theta/\partial z) / (u_* / \kappa z)^2$. Also $K_B = \kappa u_* z$. Thence, from (5a) and (5c) the components τ_B and τ of the full shear stress $\tau_s (= \tau_B + \tau)$ in the surface layer become

$$\tau_B = \kappa u_* z \frac{dU_B}{dz}, \quad (6a)$$

$$\tau = 2\kappa u_* z \frac{\partial u}{\partial z} + \frac{\kappa \hat{\alpha} g z}{\theta_0 u_*} F_\theta. \quad (6b)$$

In the surface layer the changes in shear stress and heat flux are very small compared to their surface value (i.e. $|\tau(z) - \tau(z_0)|/\tau(z_0) \ll 1$, where z_0 is the surface roughness length). Also in the surface layer

$$F_\theta = -\kappa u_* z \frac{\partial \theta}{\partial z}. \quad (6c)$$

These expressions are valid for weak stratification but are qualitatively different for strong stable stratification (see e.g. Galimiche and Hunt, 2002).

In the limit of $F_\theta = 0$, (6b) reduces to the standard form of the perturbed boundary layer with neutral stratification. Then τ_s , τ and F_θ are effectively constant with height. The results (6b), (6c) can be compared with the Monin-Obukhov similarity result for the total velocity gradient dU/dz in near neutral condition (Garratt, 1992; Townsend, 1965). It follows from (6b) (to first order in u/U_B) that, since $\tau_s^{1/2} = u_* + \tau/(2u_*)$,

$$\frac{\partial U}{\partial z} = \frac{\partial U_B}{\partial z} + \frac{\partial u}{\partial z} = \frac{\tau_s^{1/2}}{\kappa z} \left(1 - \alpha \frac{z}{L_{MO}} \right), \quad (7a)$$

where the L_{MO} is the Monin-Obukhov stability length given by

$$L_{MO} = -\frac{\tau_s^{3/2}}{\kappa(g/\theta_0)F_\theta}, \quad (7b)$$

and $\alpha = \hat{\alpha}/2$. Since field data for the atmospheric boundary layer (ABL) shows that $\alpha \approx 5$, then the coefficient $\hat{\alpha} \approx 10$. For a physical explanation and a quantitative derivation of the value of α based on the turbulence energy equation see Hunt et al. (1988).

We note that in the outer part of the boundary layer where $z \gtrsim h/10$, with h the boundary layer depth, ν_B and K_B reach a maximum value. Average values for estimating the perturbations above the surface layer are

$$\nu_B = \frac{\kappa u_* h}{10}, \quad (7c)$$

and (since $K_B \simeq 2\nu_B$ in weakly sheared flow ((Townsend, 1976)),

$$K_B \sim \frac{u_* h}{10}. \quad (7d)$$

Thence τ and F_θ can be derived as in (6b) and (6c).

To solve the time-dependent governing equations we require initial and boundary conditions. At the surface ($z = z_0$)

$$u(z_0, t) = 0, \quad (8a)$$

and

$$F_\theta(z_0, t) = 0 \quad (t < 0) \quad \text{and} \quad F_\theta(z_0, t) = F_s \quad (t > 0), \quad (8b)$$

where F_s is the constant perturbation surface heat flux initiated at $t = 0$. Far above the surface, the perturbation velocity and temperature vanish, so that, as $z \rightarrow \infty$,

$$u(z, t) = 0, \quad (8c)$$

and

$$\theta(z, t) = 0. \quad (8d)$$

3. ANALYTICAL MODELS OF PERTURBED TURBULENT BOUNDARY LAYERS

3.1. TEMPERATURE FIELD IN THE SURFACE LAYER FOR WEAK SURFACE HEAT FLUX

To first order the equation for the unsteady perturbed potential temperature (3) is decoupled from the equation for the perturbation velocity (4), whereas the equation for u is coupled to the temperature field. Therefore, we first solve for the temperature field and use these results to obtain the velocity field as described in Section 3.3. Equations (3) and (6c) are combined as:

$$\frac{\partial \theta}{\partial t} - \frac{\partial}{\partial z} \left(\kappa u_* z \frac{\partial \theta}{\partial z} \right) = 0. \quad (9)$$

We solve (9) subject to boundary conditions (8b) and (8d), noting that this model for diffusivity is only valid in the surface layer where $z/h \lesssim 1/10$.

3.2. SELF SIMILAR SOLUTION

For the particular initial conditions (8b), equation (9) can be transformed to an ordinary differential equation by combining the two dependent variables, z and t , into a single independent variable $\zeta = z/(\kappa u_* t)$ (called a similarity variable) following Townsend (1965). Also, we make θ dimensionless with respect to the given reference quantities u_* , F_s . Thence

$$\theta = \frac{F_s}{\kappa u_*} \theta^*(\zeta), \quad (10a)$$

where θ^* is the dimensionless potential temperature perturbation and

$$\zeta \frac{d\theta^*}{d\zeta} = -1 \quad \text{as} \quad \zeta \rightarrow \frac{Z_0}{\kappa u_* t} \quad \text{at the surface}; \quad \theta^* \rightarrow 0 \quad \text{as} \quad \zeta \rightarrow \infty. \quad (10b)$$

Then (9) reduces to

$$\zeta \frac{d^2 \theta^*}{d\zeta^2} + (\zeta + 1) \frac{d\theta^*}{d\zeta} = 0. \quad (11)$$

The solution to (11) subject to boundary condition (10b) is

$$\theta(\zeta) = \frac{F_s}{\kappa u_*} E_1(\zeta), \quad (12a)$$

where E_1 is the exponential integral defined as

$$E_1(\zeta) = \int_{\zeta}^{\infty} \frac{\exp(-\zeta')}{\zeta'} d\zeta'. \quad (12b)$$

The perturbation heat flux F_{θ} is therefore given by

$$F_{\theta}(\zeta) = F_s \exp(-\zeta). \quad (13)$$

Since as $\zeta \rightarrow \infty$, $E_1(\zeta) = \exp(-\zeta)/\zeta$, the temperature profile at the top of the thermal layer is

$$\theta(\zeta) = \frac{F_s}{\kappa u_* \zeta} \exp(-\zeta) \quad \text{for } \zeta \gg 1. \quad (14)$$

Since as $\zeta \rightarrow 0$, $E_1(\zeta) \sim -(\gamma + \ln(\zeta))$ (with $\gamma = 0.57721$ the Euler's constant), the temperature profile near the ground is given by the usual logarithmic profile

$$\theta_s - \theta(z, t) = \frac{F_s}{\kappa u_*} \ln\left(\frac{z}{z_0}\right), \quad (15)$$

where the surface temperature θ_s is given by

$$\theta_s = \frac{F_s}{\kappa u_*} \left[\ln\left(\frac{\kappa u_* t}{z_0}\right) - \gamma \right]. \quad (16)$$

Thus, θ_s initially increases logarithmically (at this time the thickness l_{θ} is small).

When the thermal layer thickness, l_{θ} , is greater than the surface layer thickness, h_s ($\sim h/10$), i.e. $l_{\theta} > h_s$ (or $u_* t/z_0 > h_s/z_0$), the thermal layer spreads into the upper part of the boundary layer where $K_B \sim 0.1 u_* h$. Then the similarity solution takes on the standard form of a Gaussian plume and l_{θ} grows more slowly with time as the heat flux heats a thicker layer, so that $l_{\theta} \sim \sqrt{0.1 u_* h t}$ and θ_s increases in proportion to $t^{1/2}$ as

$$\theta_s \sim \sqrt{\frac{10 t u_* F_s}{h}} \frac{F_s}{u_*}. \quad (17)$$

Eventually when the thermal layer fills the boundary layer when $t \gtrsim t_B$, where $t_B = h/u_*$, the 'plume' is limited to the boundary layer depth and $l_{\theta} \sim h$, and θ_s increases linearly with time, so that

$$\frac{\theta_s u_*}{F_s} \sim \frac{u_*(t + t_B)}{z_0} \frac{h}{z_0}. \quad (18)$$

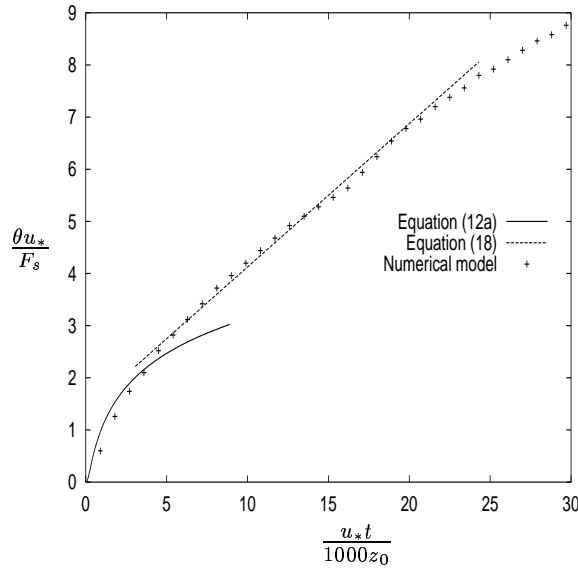


Figure 2. The time variation of the potential temperature perturbation at $z = 10$ m calculated for a neutral surface layer (with no dynamics) using (12a) and (18) for weak cooling of magnitude $F_s = -0.02 \text{ Kms}^{-1}$ imposed at $t = 0$. Also shown are results from the numerical model (UM 4.5; which includes dynamics), which are discussed in Section 4. Here $z_0 = 0.1 \text{ m}$ and $u_* \approx 0.3 \text{ ms}^{-1}$. Note that significant dynamical changes occur for $u_* t_{MO}/z_0 = L_{MO}/10z_0 \gtrsim 100$.

Figure 2 shows results of (12a) and (18) for the variation of the perturbation potential temperature at 10 m with time ($t > 0$) for weak cooling of magnitude $F_s = -0.02 \text{ Kms}^{-1}$ (or approximately -20 Wm^{-2}) imposed at $t = 0$.

Note that in these calculations u_* is assumed constant. However, as we show in the next section when $t \gtrsim t_{MO}$, with t_{MO} the Monin-Obukhov time-scale, the shear stress is significantly increased/reduced for heated/cooled surfaces, and u_* varies accordingly.

3.3. VELOCITY PERTURBATION IN THE SURFACE LAYER WITH WEAK SURFACE HEAT FLUX

Given the perturbation temperature θ , we make use of (6b) and (12a) to solve (4), subject to (8a) and (8c), for the perturbed velocity field u in the surface layer. The temperature and the forcing terms for u have a similarity form defined in terms of F_s/u_* and t_{MO} , defined here as

$$t_{MO} = \left(\frac{\kappa \hat{\alpha} g |F_s|}{\theta_0 u_*^2} \right)^{-1} \approx \frac{|L_{MO}|}{10u_*}. \quad (19a)$$

This is the time-scale on which any surface perturbations diffuse vertically over the Monin-Obukhov scale (for the equivalent equilibrium boundary layer) defined from (7b) as

$$L_{MO} = -\frac{u_*^3 \theta_0}{\kappa g F_s}. \quad (19b)$$

It follows that the solution for (4) is in the form

$$u = u_* \left(\frac{t}{t_{MO}} \right)^q \text{sgn}(F_s) G_u(\zeta, \zeta_0), \quad (19c)$$

where the exponent q is such that the resulting ordinary differential equation is independent of t and $\text{sgn}(F_s)$ is the sign of F_s . This form of solution balances the main terms of (4), so that $\partial u / \partial t \propto F_\theta$. Since near the surface $F_\theta \sim \text{constant}$, $\partial u / \partial t \propto \text{constant}$, and therefore $u \propto t$. The appropriate differential equation is obtained with $q = 1$ of the form

$$2\zeta \frac{d^2 G_u}{d\zeta^2} + (\zeta + 2) \frac{dG_u}{d\zeta} - G_u = -\zeta \frac{d\hat{F}_\theta}{d\zeta} - \hat{F}_\theta(\zeta), \quad (20)$$

where the normalized heat flux $\hat{F}_\theta = F_\theta / F_s$, where \hat{F}_θ is given by $\hat{F}_\theta = \exp(-\zeta)$. Thus

$$2\zeta \frac{d^2 G_u}{d\zeta^2} + (\zeta + 2) \frac{dG_u}{d\zeta} - G_u = (\zeta - 1) \exp(-\zeta). \quad (21)$$

The general solution for (21) is

$$G_u = A_1 \left[(\zeta + 2) E_1 \left(\frac{\zeta}{2} \right) - 2 \exp \left(-\frac{\zeta}{2} \right) \right] + A_2 (\zeta + 2) + 2(\zeta + 2) E_1(\zeta) - \exp(-\zeta), \quad (22)$$

where A_1 and A_2 are unknown coefficients of the complementary function to be determined from boundary conditions. The coefficient $A_2 = 0$ so as to satisfy (8c) as $\zeta \rightarrow \infty$. A_1 is determined by the surface boundary layer condition (8a) so that $G_u(\zeta) = 0$ at $\zeta = \zeta_0 = z_0 / (\kappa u_* t)$. Therefore equation (22) for small ζ can be written as

$$G_u(\zeta) = -(2A_1 + 4) \ln \zeta + (2 \ln 2 - 2 - 2\gamma) A_1 - (4\gamma + 1), \quad (23a)$$

with

$$A_1 = -\frac{4\gamma + 4 \ln \zeta_0 + 1}{2(\gamma + \ln \zeta_0 - \ln 2 + 1)}. \quad (23b)$$

Since for $t \gg z_0 / u_*$, $\zeta_0 \rightarrow 0$ and $\ln \zeta_0 \rightarrow -\infty$, we can approximate (23b) by

$$A_1 \approx -2 \left(1 + \frac{\lambda}{\ln \zeta_0} \right), \quad (23c)$$

where $\lambda = \ln 2 - 3/4 = -0.057$. Hence, in (22)

$$G_u(\zeta) \approx 2(\zeta + 2) \left[E_1(\zeta) - E_1\left(\frac{\zeta}{2}\right) \right] + 4 \exp\left(-\frac{\zeta}{2}\right) - \exp(-\zeta) - \frac{2\lambda}{\ln \zeta_0} \left[(\zeta + 2) E_1\left(\frac{\zeta}{2}\right) - 2 \exp\left(-\frac{\zeta}{2}\right) \right]. \quad (24)$$

Thus

$$G_u \sim -\frac{16 \exp(-\zeta/2)}{\zeta^2} < 0 \quad \text{as } \zeta \rightarrow \infty, \quad (25a)$$

while

$$G_u \sim 4\lambda \left(\frac{\ln \zeta}{\ln \zeta_0} - 1 \right) = 0.23 \left(1 - \frac{\ln(\kappa u_* t/z)}{\ln(\kappa u_* t/z_0)} \right) > 0 \quad \text{as } \zeta \rightarrow \zeta_0, \quad (25b)$$

and

$$G_u = 0 \quad \text{at } \zeta = \zeta_0. \quad (25c)$$

Figure 3(a) shows similarity profiles of $G_u(\zeta)$ computed using (24) for various values of $\zeta_0 = z_0/(\kappa u_* t)$. It shows that G_u has one maximum ($G_{u\max}$) and one minimum value ($G_{u\min}$) between $\zeta = \zeta_0$ and $\zeta \rightarrow \infty$. For typical values of z_0 and t , $G_{u\max}$ lies in the range 0.1 to 0.15 at a value of $\zeta \approx 0.1$. $G_{u\min}$ is approximately 0.03. Note that the maximum value of G_u occurs at a value of ζ , ζ_{\max} , that varies approximately with ζ_0 as

$$\zeta_{\max} \sim \frac{1}{\ln(1/\zeta_0)}. \quad (26a)$$

In physical terms this level z_{\max} rises with time in proportion to

$$z_{\max} \sim \frac{\kappa u_* t}{\ln(\kappa u_* t/z_0)}. \quad (26b)$$

In the upper part of the thermal layer the minimum negative value of G_u occurs at a constant value of ζ , independent of ζ_0 . In physical terms this level z_{\min} is

$$z_{\min} \sim 2.3 \kappa u_* t. \quad (27a)$$

Thence u_{\min} is given as

$$u_{\min} \approx \frac{t}{t_{MO}} u_* \text{sgn}(F_s). \quad (27b)$$

Equation (25b) shows that very near the surface the perturbation velocity has a log profile (provided $l_\theta \gg z_0$),

$$u \sim 0.23 u_* \frac{t}{t_{MO}} \frac{\ln(z/z_0)}{\ln(\kappa u_* t/z_0)} \text{sgn}(F_s). \quad (28)$$

This expression is equivalent to the results of Townsend (1965) (for weak stratification) for the velocity profile near the ground. (His analysis did not account for the distorted perturbation profiles where $z \sim l\theta$.)

Figure 3(b) shows the time variation $u/u_* = (t/t_{MO})\text{sgn}(F_s)G_u(\zeta)$ with height, computed using (19c) and (24) for various values of t/t_{MO} and a weak surface cooling of $F_s = -0.02 \text{ Kms}^{-1}$, $z_0 = 0.1 \text{ m}$ and $u_* = 0.3 \text{ ms}^{-1}$. A distinct maximum in the perturbation velocity, i.e. a wind jet, is evident which increases in height time. Note that the sign of the velocity perturbation is changed when the surface is heated ($F_s > 0$). Since $U = U_B + u$, it follows from the monotonically increasing form of U_B that for weak surface heat flux wind jets occur only when the surface is cooled!

To leading order, only $\partial\theta/\partial z$ affects the Richardson number Ri , which is given by

$$|Ri| = \frac{g}{\theta_0} \frac{|\partial\theta/\partial z|}{(\partial U_B/\partial z)^2} = \frac{g|F_s|z^2}{u_*^4\theta_0 t} \frac{d\theta^*}{d\zeta}, \quad (29a)$$

so that from (12a) at the top of the boundary layer where $z \sim \kappa u_* t$

$$|Ri| = \frac{t}{t_{MO}} \frac{\kappa}{2\alpha} \frac{\exp(-\zeta)}{\zeta} \sim \frac{1}{\hat{\alpha}} \frac{t}{t_{MO}}. \quad (29b)$$

Thus the modulus of the Richardson number $|Ri|$ steadily increases with time. When $t \sim \hat{\alpha} t_{MO}$, $|Ri| \sim 1$. Then the stratification is so strong that the perturbation theory developed here becomes invalid.

Substituting u (from (19c)) and F_θ (from (13)) into (6b) leads to the similarity profile of the perturbation shear stress,

$$\tau = \kappa u_*^2 \frac{t}{t_{MO}} G_\tau(\zeta), \quad (30a)$$

where

$$G_\tau(\zeta) = 2\zeta \frac{\partial G_u}{\partial \zeta} + \zeta \exp(-\zeta). \quad (30b)$$

Note that from (28), at the surface

$$\frac{\tau}{\tau_s(t=0)} = \left(\frac{2\kappa z}{u_*} \frac{\partial u}{\partial z} \right)_{z \rightarrow 0} = 0.18 \frac{t}{t_{MO}} \text{sgn}(F_s) \ln \left(\frac{t}{t_{MO}} \frac{L_{MO}}{z_0} \kappa \hat{\alpha} \right). \quad (30c)$$

Thus, for typical weakly stratified boundary layer with $u_* \sim 0.1 \text{ ms}^{-1}$, $h \sim |L_{MO}| \sim 10^3 \text{ m}$, and $t_{MO} \sim |L_{MO}|/10u_* \sim 1000 \text{ s}$, it follows from (30c) that $t/t_{MO} \gtrsim 1$ or $t > 10^3 \text{ s}$ before the surface shear stress is significantly affected by the surface heating/cooling and for $|Ri|$ (given

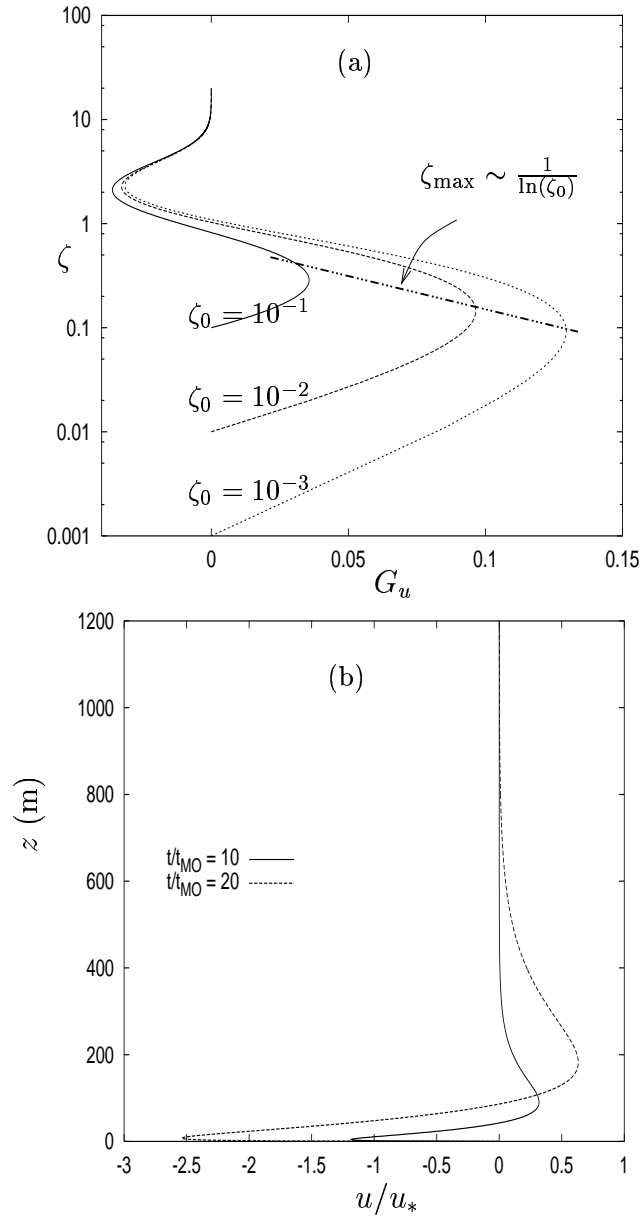


Figure 3. Perturbation velocity profiles (u) calculations for abruptly heated/cooled surfaces. (a) Similarity profiles, $G_u(\zeta)$, given by (24) for various values of $\zeta_0 = z_0/(\kappa u_* t)$. Note that as $\zeta \rightarrow \zeta_0$ there is a log profile. (b) Time variation of $u/u_* = (t/t_{MO})\text{sgn}(F_s)G_u(\zeta)$ for a weak surface cooling of $F_s = -0.02 \text{ Kms}^{-1}$. Here $z_0 = 0.1 \text{ m}$ and $u_* = 0.3 \text{ ms}^{-1}$. Note $u_* t_{MO}/z_0 = L_{MO}/10z_0 \sim 100$.

by (29a)) to change. But with moderate stratification where L_{MO} is reduced to 10^2 m, the time is reduced to approximately 10^2 s, about the time for heat to diffuse through the surface layer.

Although the model is valid only in the surface layer of the boundary layer (where $z \lesssim 100$ m), the qualitative forms of the perturbation profiles τ , $\partial\tau/\partial z$, θ and u are similar in the upper part of the layer. This can be demonstrated in the limit when $t \gg h/u_*$ so that the perturbed thermal layer has filled the boundary layer (assuming no diffusion above it). Then

$$\theta \rightarrow \frac{tF_s}{h} \quad \text{and} \quad F_\theta \simeq F_s \left(1 - \frac{z}{h}\right).$$

The perturbation shear stress (6b) becomes

$$\tau \approx \frac{2\kappa u_* z}{(1+z/h)} \frac{\partial u}{\partial z} + \frac{u_* z}{t_{MO}} \left(1 - \frac{z}{h}\right). \quad (31)$$

It is clear that the thermal forcing term is of the same form as in the surface layer, leading to a velocity perturbation from (4) similar to that of the surface layer solution, namely (for $z \gtrsim h/10$) the perturbation velocity decreases towards the top of the boundary layer, i.e.

$$u \approx u_* \frac{t}{t_{MO}} \left(1 - \frac{2z}{h}\right). \quad (32)$$

However, when $t \sim \hat{\alpha}t_{MO}$, it follows from (29b) that this predicted growth of the velocity perturbation is invalid. Then the modulus of the Richardson number $|Ri| \sim 1$ and the turbulence in the boundary layer changes significantly from its initial state in the neutrally stratified boundary layer.

3.4. PERTURBATION OF THE CONVECTIVE BOUNDARY LAYER

The above analysis can be extended to estimate the adjustment of the above neutral boundary layer with velocity $U_B(z)$ when it is perturbed by strong thermal convection being imposed at $t > 0$. In general the transition persists for long enough that Coriolis forces are significant. We also consider briefly the effect of adjustment with spatially varying surface heat fluxes.

3.4.1. *Strong surface heat flux*

Following the analysis of Hunt et al. (1988, 2003a), if the heating applied at $t = 0$ is strong enough that $h/|L_{MO}| \gg 1$, the root mean square turbulent velocity (u') is determined by the buoyancy forces, so that, for

$t > \hat{\alpha}t_{MO}$, $u' \sim w_*$, where $w_* \sim (gF_s h/\theta_0)^{1/3}$. The convection timescale h/w_* is smaller than the shearing timescale h/u_* , and the mean shear generates Reynolds stresses (Rao and Narasimha, 1996). The convective eddy viscosity in the surface layer is $\nu_e \sim Pr_t \sigma_w z \sim Pr_t w_* (z/h)^{1/3} z$ (c.f. Wyngaard and Brost (1984) estimated the z exponent as $3/2$, a difference which does not affect the form of the result). Here Pr_t is the turbulent Prandtl number ($\simeq 0.4$) for isotropic turbulence; it may be smaller for eddies with large vertical structures in turbulent convection (Townsend 1976, Chapter 8). Therefore the total shear stress associated with convection (denoted as τ_c) is determined by

$$\frac{\partial \tau_c}{\partial z} \sim \frac{\partial}{\partial z} \left(\frac{Pr_t w_* z^{\frac{4}{3}}}{h^{\frac{1}{3}}} \frac{\partial(U_B + u)}{\partial z} \right) \sim \frac{Pr_t w_* u_*}{z^{\frac{2}{3}} h^{\frac{1}{3}}} \quad \text{for } z \ll h. \quad (33a)$$

But in the middle/upper part of the layer, where the eddy viscosity is approximately constant

$$\frac{\partial \tau_c}{\partial z} \sim \frac{\partial}{\partial z} \left(Pr_t w_* h \frac{\partial(U_B + u)}{\partial z} \right) \sim -\frac{Pr_t w_* u_*}{h} \quad \text{for } z \sim h. \quad (33b)$$

Note that the negative sign is associated with the negative value of $d^2 U_B/dz^2$ ($\sim -u_*^2/h$). The result (33a) shows that in the surface layer when $t > t_{MO}$, the gradient of the convective shear stress continues to amplify the surface velocity perturbation, following the initial linear phase when $t < t_{MO}$. Substituting the convective shear stress gradient (33a) into (4) provides an estimate of the growth of u . Near the surface

$$\frac{u}{u_*} \sim Pr_t \frac{t}{t_{MO}} \frac{w_*}{u_*} \left(\frac{z}{h} \right)^{-\frac{2}{3}} \left(\frac{h}{L_{MO}} \right)^{-1} = \frac{Pr_t t w_*}{h} \frac{1}{(z/h)^{\frac{2}{3}}}, \quad (34a)$$

and in the middle/upper part of the boundary layer

$$\frac{u}{u_*} \sim -\frac{Pr_t t w_*}{h}. \quad (34b)$$

(These are upper estimates because the shear stress induced by $\partial u/\partial z$ is neglected, and break down when $u_* \sim w_*$.)

The complex role of the shear stresses in these flows is demonstrated by experiments and numerical simulations (Section 5), which are consistent with the calculation (34a) that strong convection can drive a steady state mean shear flow or greatly reduce the effects of surface friction that tend to slow it down. Note that the shear stress generated by the mean shear, i.e. τ_s , decreases with z in the surface jet. However the large convective eddies or plumes as they rise through the surface shear flow also contribute a convective component to the shear stress τ_c

(as in (33a)). Effectively, τ_c drives the flow as result of the distortion of the eddies by the shear, as in the ‘moving flame experiment’ (e.g. Hinch and Schubert (1971)). This leads to τ_c increasing with z . However, the growth of the mean shear induces small scale eddy motions and a shear stress τ_s proportional to the local shear, i.e. $\tau_s \propto \partial U/\partial z$, with the opposite sign to $\partial\tau_c/\partial z$. Thus, the mean velocity can be close to equilibrium (in which case $\partial\tau_s/\partial z + \partial\tau_c/\partial z = 0$) or may decay slowly over a long time-scale of the order βt_A that is large compared to the natural convective time-scale

$$t_A = \frac{h}{w_*} \sim \frac{h/u_*}{(h/|L_{MO}|)^{1/3}}. \quad (35a)$$

(Numerical simulations indicate that β may be as large as 10 when strong heating is suddenly applied. See Section 5). Note that t_A is the relaxation time, over which the ratio $\partial u/\partial t/\partial\tau/\partial z$ becomes very small, and the mean velocity adjusts to its final state. By comparison the buoyancy shear time-scale introduced in (19a) is $t_{MO} = |L_{MO}|/(10u_*)$, which is the time over which heat is diffused vertically over the Monin–Obukhov length, and also, as we have shown by our analysis previously, the time for the Richardson number Ri in the thermal layer to change. Note that the convective time-scale t_A becomes significantly greater than t_{MO} as the stratification becomes stronger. From (35a) and (19a)

$$\frac{t_{MO}}{t_A} \sim \left(\frac{h}{|L_{MO}|} \right)^{-\frac{2}{3}}. \quad (35b)$$

However, when $h/|L_{MO}| \gg 1$, t_A is significantly smaller than the natural shear time-scale of the neutral boundary layer, namely $t_* = h/u_*$. In strong convection, e.g. when $h/|L_{MO}| \sim 10^2$, (35b) shows that the slow decay time βt_A may be comparable with t_* . By contrast if the heating is weak enough that $h/|L_{MO}| \lesssim 1$, the perturbation velocity caused by thermal effects is weak, i.e. u/u_* is small. It is observed that in these situations the flow adjusts monotonically to its asymptotic steady state without any overshoots and jets developing in the profiles.

Similar qualitative variation in the perturbations occur when the surface is cooled sufficiently fast. In this situation the turbulence is damped by stable buoyancy forces so that u/u_* steadily decreases. The temperature gradient increases and at the height of the thermal boundary layer the velocity gradient decreases, so that for $t \sim t_*$, $Ri \gtrsim Ri_{\text{crit}}$ where the critical Richardson number Ri_{crit} is about equal to 0.3 ± 0.05 .

This means that the turbulent diffusion and also shear stress in the thermal layer decrease to zero. Thus at $z \sim l_\theta$, for $t > t_{MO}$, $\tau + \tau_B = 0$ or

$\tau = -\tau_B$. The solution to (2a) shows that in the upper part of the thermal layer the velocity accelerates since $\partial\tau/\partial z = -\partial\tau_B/\partial z > 0$. This could explain the large formation of wind jets over cooled surfaces. But the acceleration and increased velocity gradients lead to *Ri* decreasing. Turbulence may be amplified with a consequent slowing down of the layer. The observed oscillatory behaviour of stable boundary layers on time-scales of order h/u_* might be explained by this mechanism (Derbyshire, 1994). In other words, if $h/|L_{MO}| \gg 1$, the neutral or convective boundary layer when cooled may not always tend monotonically towards a fully developed stably stratified boundary layer. As commonly observed in the tropical evening when a stagnant layer occurs below 30 m (Singal *et al.*, 1985).

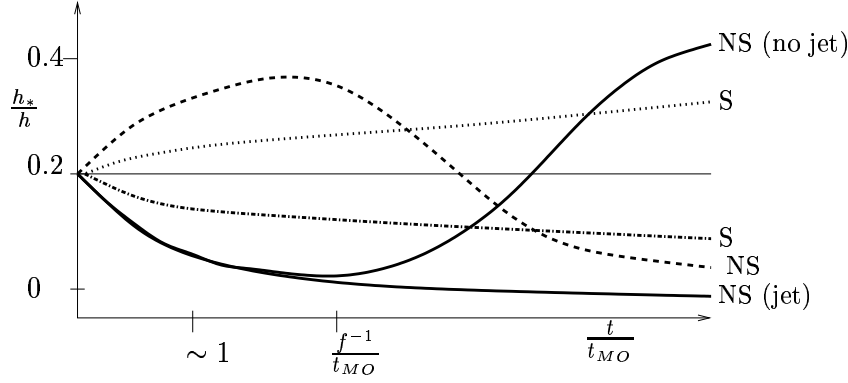
A suitable measure for how the mean velocity profiles change is the ratio of the displacement thickness h_* to the boundary layer thickness h , where

$$h_* = \int_0^\infty \left(1 - \frac{U}{U_\infty}\right) dz, \quad (36)$$

and U_∞ is the value of U as $z \rightarrow \infty$ (i.e. $z \sim L$) and h is defined as where $U \simeq 0.99U_\infty$. Note that $h_*/h \sim 0.2$ for a typical neutral boundary layer (NBL) (Garratt, 1992). Summarising the standard results, h_*/h changes to become less/greater than in the NBL if the heating/cooling is weak and slow, corresponding to boundary layer profiles becoming flatter or more sheared. However, if the heating is rapid and either weak or strong, then from the results presented here h_*/h initially increases. But for larger times (as the following section demonstrates) when $t \sim 1/f > t_{MO}$, h_*/h tends to its value for equilibrium boundary layers which is less than in the NBL. Finally, if the cooling is strong and rapid, then h_*/h takes a very long time ($\sim \beta t_A$) before tending to its limit. This can be either greater/less than in the NBL depending on whether there are no jets/jets. There may be situations where it does not occur. Figure 4 sketches the evolution of the profile parameter h_*/h against t/t_{MO} for boundary layers as they are heated/cooled rapidly or slowly.

3.4.2. *Effects of Coriolis acceleration*

Since it has been widely suggested that the maxima in the wind profiles are caused by the combination of surface cooling and Coriolis acceleration (Blackadar, 1957; Smedman *et al.*, 1995), it is interesting to test this idea for the idealised flow considered here. Since the time-scale for the Coriolis effect $1/f$ ($\sim 10^4$ s) is much larger than the time-scale for the thermal layer to fill the boundary layer ($h/u_* \sim 10^3$ s). It follows from (33a) and (33b) that (ignoring shear stresses as in (32) because



- Rapid, surface heating (weak or strong) ($t_\theta \lesssim t_{MO}$).
- Slow, weak surface cooling ($t_\theta/t_{MO} \gg 1$; $h/|L_{MO}| \lesssim 1$).
- .-.-.- Slow, weak surface heating ($t_\theta/t_{MO} \gg 1$; $h/|L_{MO}| \lesssim 1$).
- Rapid, strong surface cooling ($t_\theta \lesssim t_{MO}$; $h/|L_{MO}| \gg 1$).

Figure 4. A sketch of how heated or cooled boundary layers evolve to their final state depending on the rate of growth of heating or cooling determined by t_θ/t_{MO} . Note that h_* is the displacement thickness defined by (36). S and NS denotes ‘standard’ slow and ‘non-standard’ (rapid) asymptotic states. Here $(h_*/h)_{\text{NBL}} \sim 0.2$.

they do not affect estimates of adjustment time)

$$\frac{\partial u}{\partial t} = fv + \frac{u_*}{t_{MO}} \text{sgn}(F_s) \left(1 - \frac{2z}{h}\right) \mathcal{H}(tf) + \mathcal{O}\left(\kappa u_* h \frac{\partial^2 u}{\partial z^2}\right), \quad (37a)$$

$$\frac{\partial v}{\partial t} = -fu + \mathcal{O}\left(\kappa u_* h \frac{\partial^2 v}{\partial z^2}\right). \quad (37b)$$

Here \mathcal{H} is the Heaviside step function and v is the velocity perturbation in the crosswind direction. (Note that the perturbation horizontal pressure gradients are negligible above, and therefore within, the thermal layer.) Thence the approximate governing equation for u (ignoring the perturbation shear stresses which further damp the velocity perturbation) is

$$\frac{\partial^2 u}{\partial t^2} + f^2 u = \frac{u_* \delta(tf) f}{t_{MO}} \text{sgn}(F_s) \left(1 - \frac{2z}{h}\right), \quad (38a)$$

where $\delta()$ is the delta function. The solution is

$$u = \frac{u_*}{f t_{MO}} \sin(tf) \text{sgn}(F_s) \left(1 - \frac{2z}{h}\right). \quad (38b)$$

This shows that the Coriolis effect reduces and even reverses the maximum velocity, rather than generating the buoyancy induced perturbation; the maximum positive or negative value of u is

$$|u|_{\max} = \frac{u_*}{ft_{MO}}. \quad (39)$$

We note from (38b) that the wind jet usually occurs with cooling at the surface and is located near the top of the boundary layer. Note that Coriolis effects limit the growth of the velocity perturbation (and the variation of h) as follows from the momentum equation,

$$\frac{\partial h_*}{\partial t} = \frac{\tau(z=0) - f \int_0^\infty v dz}{U_\infty}. \quad (40)$$

Thus if the Coriolis force is present h_* tends to asymptote to a constant value that maybe higher or lower than the value in the NBL.

It is important to note that observational data by Bonner (1968) does not show inertial oscillations which Blackadar (1957) suggests is as a result of the effect of the Coriolis force on accelerating air flow.

3.4.3. *Spatially varying surface heat flux*

When these concepts are applied to spatial variation in heating or cooling with a boundary layer wind U_B over a length scale L , so that in (2a) $\partial u/\partial t \approx U_B \partial u/\partial x$, it shows that wind jets are likely over coastal or urban areas where there are moderate thermal contrasts and $h/|L_{MO}| \gtrsim 1$. For example, when the air moves over a cool sea from warmer land, or vice versa. Typically the rate of change of cooling is on a time-scale $t_\theta \sim L/U$, which is of order h/u_* . This is why the boundary layer flow does not adjust its final unstable or stable state asymptotically and wind jets are observed in coastal areas.

4. Comparison with Numerical Simulations for Weak/Strong Surface Heat Flux

In this section numerical simulations are performed using the atmospheric NWP code the UK Met Office Unified Model, version 4.5 (UM 4.5). Initially the case of weak cooling was studied in order to compare with the results of the theoretical model for the surface layer (see Figure 3(b)). This comparison can only be approximate because the NWP code has a finite horizontal and vertical resolution. Simulations are performed also for stronger and more physically significant cooling and heating, when the theoretical model is no longer valid.

4.1. MODEL DESCRIPTION

UM 4.5 implements a non-linear, hydrostatic set of dynamical equations on a horizontal latitude-longitude grid. A Lorenz grid is used in the vertical with a ‘hybrid’ sigma/pressure coordinate system giving increased resolution near the ground and the troposphere. Cullen (1993) provides a description of the numerical formulation of the model. The physical parameterizations include schemes to represent boundary layer mixing, convection, precipitation, surface exchange, cloud formation, and shortwave and longwave radiation Clark and Hopwood (2001). The boundary layer physics employs a first order scheme which models fluxes of momentum, moisture and heat in terms of stability calculated from the local bulk Richardson number, mixing lengths, and the vertical wind shear. Mixing lengths vary with height and are based on surface roughness length and asymptotic neutral mixing lengths proportional to the boundary layer height. Surface turbulent fluxes are formulated as bulk formulae in a constant-flux surface layer and are treated using a conventional drag coefficient approach (Clark and Hopwood, 2001).

The idealised mode comprises a 146 by 182 xy -grid with a horizontal resolution of 12 km and 38 levels in the vertical. The boundary layer was modelled by the first 14 vertical levels with the lowest level at 10 m. The terrain is a flat land surface. In this idealised mode the model is run with a prescribed surface heat flux. This was achieved by constraining the latent heat fluxes and radiative heat fluxes between model levels to be zero, therefore making the heating throughout the atmosphere controlled by the choice of the surface sensible heat flux. The simulations were driven by a large-scale pressure gradient (Cullen et al., 1993), calculated for a geostrophic wind of magnitude $U_G = 7\text{ms}^{-1}$ aligned with the x -axis (from west to east) at a latitude of 65°N ($f = 1.3 \times 10^{-4}\text{s}^{-1}$ (meaning the time-scale for Coriolis forces to be significant is approximately 10^4 s)). The surface roughness length z_0 was set to 0.1 m and surface temperature θ_s to 293.15 K. The model was initialised by a run from the single column (1D) version of UM 4.5.

Lateral boundary conditions were fixed at these initial values. Starting with no heating, the model was run forward in time until it reached a steady state (i.e. until **when the absolute differences of u and v between two adjacent time steps are less than 0.01ms^{-1} everywhere in the computational domain**). At this point (defined as $t = 0$) the frictional velocity u_* was approximately 0.3ms^{-1} and a non-zero surface heat flux is introduced.

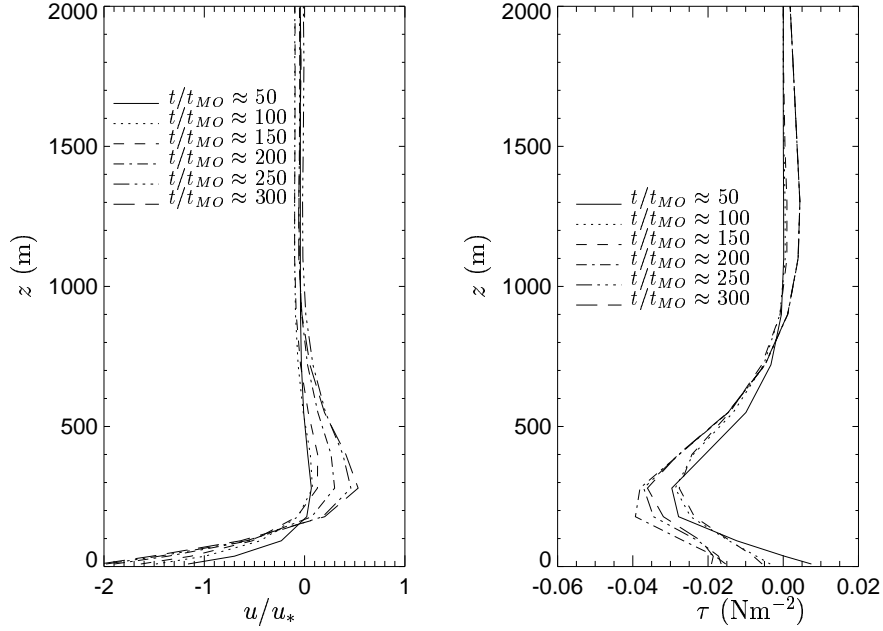


Figure 5. Time variation of the perturbation velocity profile u/u_* and perturbation shear stress profile τ computed using UM 4.5 for weak cooling of magnitude $F_s = -0.02 \text{ Kms}^{-1}$ imposed at $t = 0$. Here $f = 1.3 \times 10^{-4} \text{ s}^{-1}$, $z_0 = 0.1 \text{ m}$, $u_* \approx 0.3 \text{ ms}^{-1}$ and $\theta_s = 293.15 \text{ K}$. Note $h/|L_{MO}| \sim 3$ and $t_{MO} \approx 33 \text{ s}$.

4.2. RESULTS FOR WEAK SURFACE HEAT FLUX

A weak surface heat flux of magnitude $F_s = -0.02 \text{ Kms}^{-1}$ (i.e. $h/|L_{MO}| \sim 3$ and $t_{MO} \approx 33 \text{ s}$) was introduced at $t = 0$ to the model. Figures 2 and 5 presents the perturbation temperature and velocity profiles and the perturbation shear stress profile τ , taken from the center of the domain and for increasing values of t ($1650 \leq t \leq 9900 \text{ s}$ or $5 \times 10^3 < tu_*/z_0 < 3 \times 10^4$ or $50 \lesssim t/t_{MO} \lesssim 300$).

Figure 2 presents the time variation of the perturbation potential temperature at 10 m computed using UM 4.5. They agree with the theoretical results. For neutrally stratified surface layer, when $u_*t/z_0 > u_*t_{MO}/z_0$ buoyancy forces begin to affect the turbulence and when $t > h/u_*$, as explained in Section 3.2, $\theta_s \propto t$ as the figure shows.

Examining the perturbation velocity profile (Figure 5(a)), a significant negative velocity perturbation is evident close to the surface ($z < 50 \text{ m}$). This increases with time. Above this level the sign of the velocity perturbation changes and a maximum or wind jet is observed which

increases with t . The height of this jet is above the surface layer at 200–400m and increases slowly for $0 < t/t_{MO} < 150$. For longer periods the height of the jet is constant. For $z > 500$ m the perturbation velocity is very small (and slightly negative). Examining the perturbation shear stress profile, from the surface it initially decreases with height (corresponding to the velocity perturbation increasing) till it reaches a minimum. At upper levels the shear stress tends to zero.

Comparing Figure 5(a) with the velocity profiles calculated by the theoretical model (see Figure 3(b)) shows that, as in Figure 2, the theoretical results and numerical simulation are qualitatively similar because the surface layer theory is only formally valid for $tu_*/z_0 < t_{MO}u_*/z_0 \sim 100$ (for this case) and $tu_*/z_0 \lesssim h_s/z_0 \sim 10^3$. Note that the magnitude of the velocity perturbations calculated by the numerical model are less than the theoretical model values. The minimum in the perturbation velocity predicted by the theoretical model close to the surface is not represented in the numerical simulations because of the grid size near the surface.

When the surface is weakly heated (i.e. $F_s = 0.02\text{Kms}^{-1}$ (or approximately 20Wm^{-2})) the sign of the velocity perturbation is changed. Near the surface the velocity increases causing a slight flattening of the mean U profile and at upper levels a small decrease in the velocity occurs (not shown). This is also consistent with the theoretical model results of Section 3.3.

The time-scale for this simulation is less than $1/f$ and therefore the perturbations are not due to Coriolis forces. However, the velocity jet in this example is almost negligible when compared to the background neutral background state. Therefore we now consider some examples of stronger heating and concentrate on the mean flow U .

4.3. RESULTS FOR MODERATE/STRONG SURFACE HEAT FLUX

A strong cooling of magnitude $F_s \approx -0.5\text{Kms}^{-1}$ (or approximately -500Wm^{-2}) ($h/|L_{MO}| \sim 75$ and $t_{MO} \approx 1.3$ s) is introduced at $t = 0$ to the model. Figure 6(a) presents the combined background and perturbation velocity U for increasing values of t ($0 \leq t \leq 10800$ s or $0 \leq tu_*/z_0 < 3.3 \times 10^4$ or $0 \leq t/t_{MO} \leq 8100$). This magnitude of cooling is typical, for example, over cold polar oceans (e.g. coastal polynyas (King and Turner, 1997)), and evening inversion over continental plains.

A distinct low-level jet is evident. Both the magnitude of the jet and its vertical position increase slowly for $0 \leq t/t_{MO} \leq 2700$. For longer periods the magnitude of the jet continues to increase, though its height remains constant. Below the jet and close to the surface ($z < 100$ m) a strong decrease in velocity is seen. Above the jet ($z >$

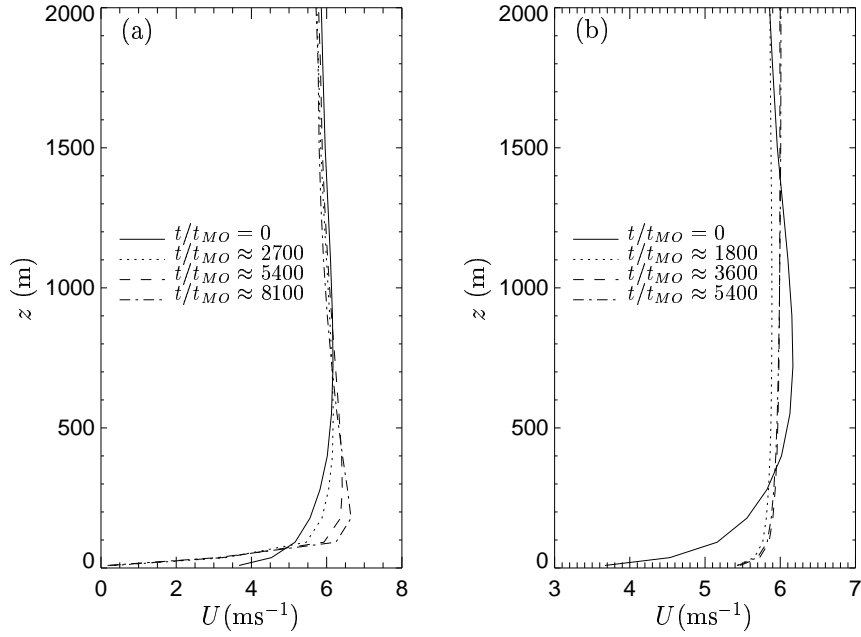


Figure 6. Time variation of $U = U_B + u$ computed using UM 4.5 for (a) strong surface cooling of $F_s \approx -0.5 \text{ Kms}^{-1}$ and (b) moderate surface heating of $F_s \approx 0.35 \text{ Kms}^{-1}$, imposed at $t = 0$. Here $f = 1.3 \times 10^{-4} \text{ s}^{-1}$, $z_0 = 0.1 \text{ m}$, $u_* \approx 0.3 \text{ ms}^{-1}$ and $\theta_s = 293.15 \text{ K}$. Note in (a) $h/|L_{MO}| \sim 75$ and $t_{MO} \approx 1.3 \text{ s}$, and in (b) $h/|L_{MO}| \sim 50$ and $t_{MO} \approx 2 \text{ s}$.

500 m) the velocity decreases slightly. Comparing with Figure 5 shows that for both weak and strong cooling the behaviour is qualitatively similar.

Figure 6(a) is qualitatively similar to the low-level jet observed by Smedman *et al.* (2004) over a land-sea transition over the Baltic Sea and over New Delhi in the evening when there is a 10° temperature fall between 1 and 30 m above the ground (Garg *et al.*, 2004). Though in Smedman's case it was proposed that the jet was due to a combination of Coriolis effects and spatial variation in heat flux. Also evident in Figure 6(a) is the presence of strong shear at low levels which Smedman also observed.

Figure 6(b) presents equivalent profiles of U when moderate surface heating of magnitude $F_s \approx 0.35 \text{ Kms}^{-1}$ (or approximately 350 Wm^{-2}) ($h/|L_{MO}| \sim 50$ and $t_{MO} \approx 2 \text{ s}$) is introduced (for $0 \leq t \leq 10800 \text{ s}$ or $0 \leq tu_*/z_0 < 3.3 \times 10^4$ or $0 \leq t/t_{MO} \leq 5400$). A large speed-up near the surface and slight decrease in velocity at upper levels is evident. This combination produces a marked flattening of the velocity profile

from its initial logarithmic shape. This magnitude of heating is typical, for example, over a forest or grassland.

Due to technical difficulties in the UM 4.5 Fortran code it was not possible to apply the numerical model to conditions of strong heating (i.e. $h/|L_{MO}| \sim 10^2$).

5. Experiments and Simulations

The theoretical and numerical model results showed that for a weak to moderate heating a flattening of the profile occurs, while wind jets formed with surface cooling (see Figures 3, 5 and 6). But the theoretical model showed that jets also might occur with strong heating. This section considers experimental evidence and Direct Numerical Simulations (DNS) of the behaviour of the ABL over a flat surface under conditions of strong heating.

5.1. FIELD EXPERIMENTS

Most field experiments of the ABL over a flat surface with rapidly changing heat flux have been where the heat fluxes vary spatially rather than temporally (e.g. over land-sea or rural urban transitions), or in the flow over accidentally released cold vapour cloud (Ooms and Tennekes, 1984). Usually the surface roughness length z_0 also changes at the same place as the surface heat flux (Townsend, 1965). But as (30c) shows the effects on the surface friction τ are quite different. With a rapidly changed heat flux the surface shear stress perturbation $|\tau|/u_*^2$ increases downwind, but with a sudden roughness changes this ratio is maximum at $x = 0$ and then decreases rapidly downwind! Furthermore the mean velocity profile changes are also quite different to those associated with roughness change. In the former case the perturbation profile forms a maximum and minimum at the ground and decreases, whereas in the latter these form of profiles are unchanged.

Measurements of mean velocity profiles on flat islands in the Baltic Sea situated about 20-40 km downwind of the coast demonstrate the effect of a land-sea heat flux change. A strong tendency to form wind jets (Smedman et al., 2004) is observed whether the flow is stably or unstably stratified. This is consistent with the estimate of $U/f \sim 30$ km as a settling distance and with the forms of the profiles predicted in section 3 for near neutral conditions.

In Rider et al's (1963) experiment of air flow over flat surface changing from grass to tarmac, there was a jump in roughness and heat flux. Townsend's (1965) tabulation of the experimental temperature

data, showed that its form and magnitudes were consistent with the analysis of the temperature perturbations in section 3.2. The value of $l_\theta/|L_{MO}|$ was of order unity. The results showed that the growth of l_θ was influenced by the buoyancy induced changes to the turbulence. There were no velocity profiles measured.

Mulhearn (1981) analysed field experiments of warm desert air advected over a cooler sea, over distances where $t/t_{MO} \sim 50$ (i.e. 4 to 40 km downwind). He showed that $l_\theta \sim 100\text{--}200$ m and that it grows very slowly (100 m over 1 km - consistent with Figure 5).

5.2. LABORATORY EXPERIMENTS

Previous experiments have shown how over flat surfaces steady or unsteady thermal forcing can induce significant mean motions, e.g. by heating a liquid in a long cuboid vessel (Krishnamurti and Howard, 1981) or by a moving source of heat (Hinch and Schubert, 1971). However, we have not seen any previous experiments (or numerical simulations) where significant heating (or cooling) (i.e. $h/|L_{MO}| \gg 1$) is suddenly applied to a sheared flow over a flat surface (on a time-scale much less than the turbulent diffusion time-scale h/u_*). We now describe a qualitative laboratory experiment to test the theoretical model of Section 3.4.

A cylindrical tank of radius $r = 0.28$ m was filled with water to a height $H = 0.11$ m and rotated steadily on a turntable at angular velocity $\Omega = 1/4$ rads^{-1} until the flow was in rapid body rotation. At time $t = 0$ the turntable was stopped so that a swirling flow with the main azimuthal component of velocity $U_\phi(z, t) \sim 6$ cms^{-1} was initiated. U_ϕ varied vertically with z in the boundary layer of height $h \sim 0.01$ m. Weaker radial and vertical velocity components (~ 1 cms^{-1}) were also set up by the radial pressure gradients. The Reynolds number of the boundary layer ($\text{Re} = U_\phi h/\nu \sim 6 \times 10^2$, where ν is the kinematic viscosity) was high enough for the flow to be turbulent. Figure 7(a) shows a vertical cross section of the mean azimuthal component of the flow field (averaged over 0.5 s) at $t = 1200$ s (i.e. $tU_\phi/H \sim tu_*/h \sim 10^3$). After this time the flow field has decayed to about 1/100 of its initial value which is of the order $(h/U_\phi)(U_\phi/u_*)^2$.

The experiment was repeated with the tank bottom heated to produce a strong heat flux both during the rotation of the tank and after it has stopped. Here $F_s = 0.3$ Kms^{-1} (or approximately 1200 Wm^{-2}) and $H/|L_{MO}| \sim 550$, so that $w_*/u_* \sim 5$. Figure 7(b) shows the mean azimuthal component of the flow field at $t = 1200$ s. Comparing Figure 7(b) with Figure 7(a) shows significant differences. With heating the peak velocity decays more slowly, U_θ is about ten times the value with

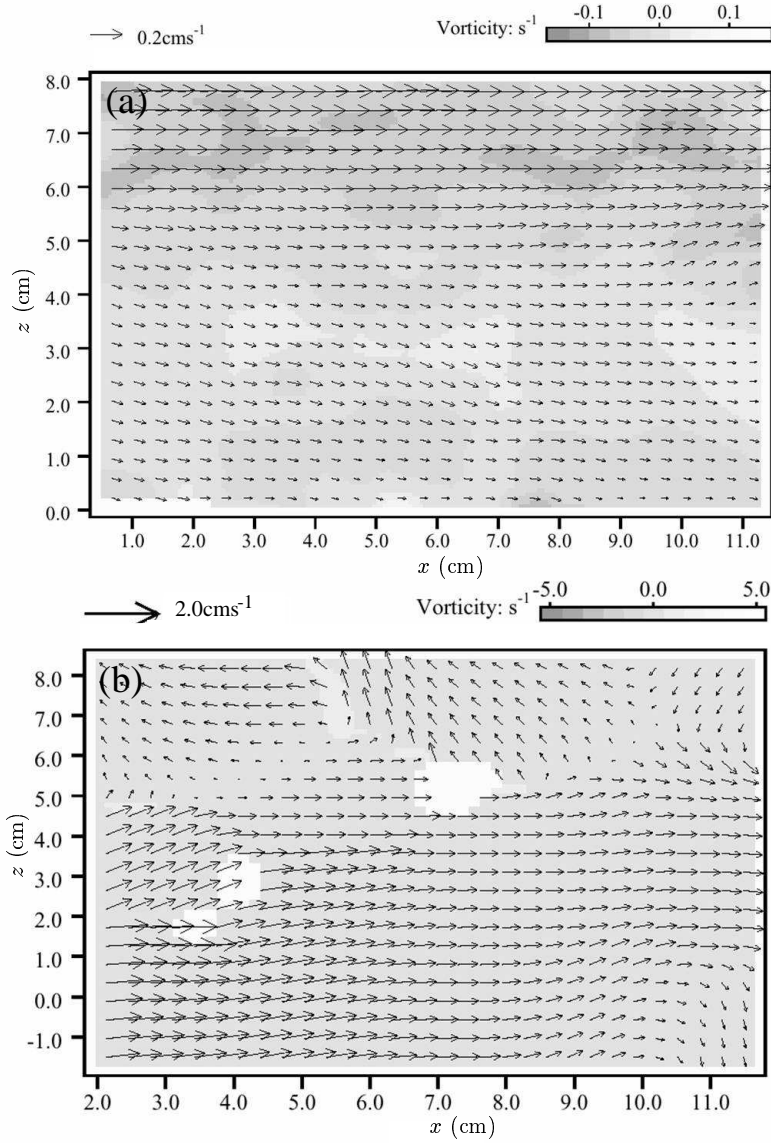


Figure 7. Vertical cross section of the azimuthal component of the flow field after $t = 1200$ s showing velocity vectors for (a) no heating ($tU_\theta/H \sim 10^3$) and (b) heating of $F_s = 0.3 \text{ Kms}^{-1}$ ($tU_\theta/H \sim 10^4$). Also shown is the vorticity. The cross-section is located at approximately $r/2$. In (a) the tank bottom is at 0.0 cm and in (b) it is at -2.0 cm. Note in (b) $H/|L_{MO}| \sim 550$ and $t/t_{MO} \approx 500000$.

no heating (i.e. $tu_*/h \sim 10^4$), and a jet forms near the bottom surface. Clearly the thermal energy is being converted into kinetic energy of the flow. This is consistent with the analysis and discussion in Section 3.4.

Flow visualisation confirmed, as expected, that the eddy structure changes from ‘horse-shoe’ vortices and streaks with no heating, characteristic of the sheared boundary layer flow (where vertical turbulence varies slowly with z), to ‘plumes’ with heating, characteristic of thermal turbulence (where vertical turbulence increases with z) (Nieuwstadt and Hunt, 2002). (These changes in rotation and eddy structure can be seen in a kitchen experiment by stirring water in a glass container and then placing it onto a heater.)

5.3. DIRECT NUMERICAL SIMULATION

The results of Section 4 showed that the UM 4.5 simulated profiles were approximately the same as the theoretical prediction, i.e. a wind jet occurs at the top of the thermal boundary layer for weak/strong surface cooling, and a flattening of the profile occurs for weak/moderate surface heating. However the code is not suitable for studying the transition of a turbulent boundary layer near the surface when the flow changes on a short time-scale (compared to $h/(10u_*) \ll 300$ s, where 300 s is the UM 4.5 time step). Additionally, due to the limited vertical resolution (38 vertical levels), the code cannot be used to study the continuous variation of the boundary layer as the heating changes from weak to very strong (i.e. $h/|L_{MO}| \lesssim 1$ increases to $h/|L_{MO}| \gg 1$). Therefore, although DNS cannot represent the profiles for a high Reynolds number ABL, their fine meshes enable vertical profiles to be accurately computed. Also their complete dynamics enable the transitions of the turbulence to be computed as $h/|L_{MO}|$ increases. The TU Delft code is used here (see Hunt *et al.*, 2003b) which has been validated for neutral, convective and stable boundary layer of height h for flow in a two-dimensional channel.

In an numerical experiment a convective turbulent layer is established with no mean flow lying between $z = 0$ and $z = h$ (with $Re \sim 400$, and Rayleigh number $Ra = 10^5$). Then a mean uniform shear $dU_B/dz \sim 5w_*/h$ is suddenly introduced at $t = 0$. The question is how rapidly (if at all) the shear changes and/or decays. The mean velocity that initially increased with height would become uniform, because, of the dynamical effects of convection in a time-scale of the order $3h/w_*$. The computation showed that the Reynold stress profile developed a peak (Figure 8a) and a jet profile was formed (Figure 8b). Note that $h/|L_{MO}| \sim 4$. This is consistent with the analysis and discussion in Section 3.4 and the original experimental finding of Krishnamurti and

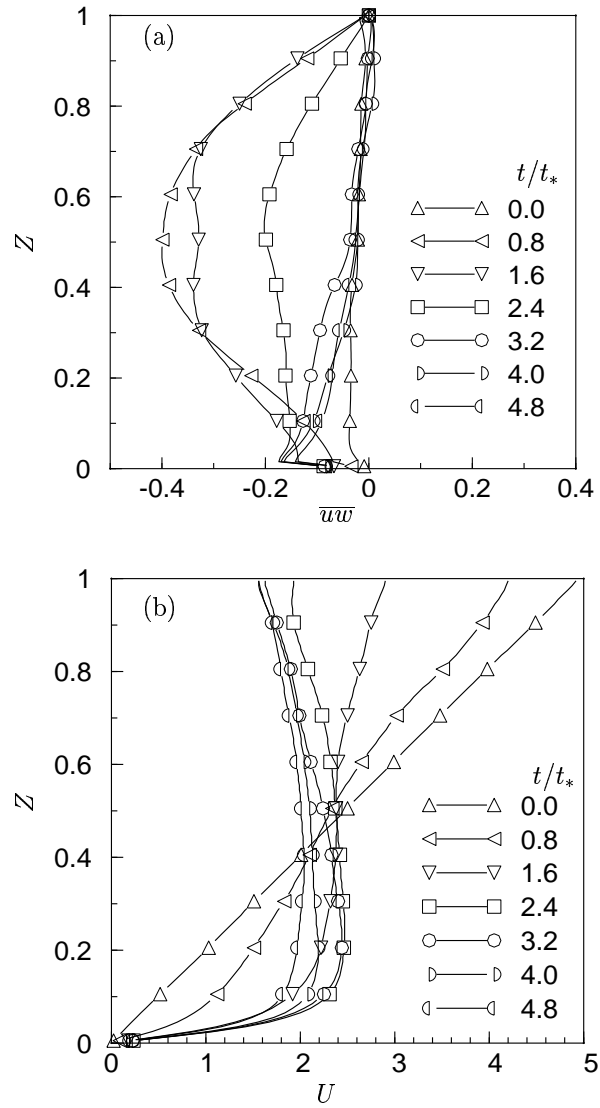


Figure 8. Decay of mean shear initiated at $t = 0$ in a convective boundary layer. Shown is the (a) Reynolds stress (scaled with w_*^2) profile and (b) mean velocity ($U = u/w_*$) profile at various values of dimensionless time $t/t_* \approx t/30t_{MO}$. The dimensionless height $Z = z/h$.

Howard (1981) that convection in a channel tends to generate a mean flow along the channel in either direction, depending on some initial perturbation. Even the mean flow is chaotic, and, in general, is not ergodic.

6. Conclusions

The theoretical, computational and experimental studies presented here show that the transitions of the ABL between fully developed states are quite complex in space and time. Any computational and theoretical models that can provide an adequate description have to be based on physical parameterisations valid for the transitional evolving states.

Nevertheless from the approximate model, experimental data, and numerical simulations, certain conclusions can be drawn about the effects of stable or unstable stratification profiles (defined by $h/|L_{MO}| \gg 1$) when they are imposed on a neutral boundary layer over a short time scale (small compared with h/u_*).

1. The changing Richardson number distorts the structure of turbulence so much that the mean velocity profiles (and surface stress) do not simply adjust to a new steady state profile (as determined by $h/|L_{MO}|$) but are altered qualitatively and take new forms. These transitional profiles typically include ‘jets’ where the mean velocity is maximum. At the early stages of the transition the peak values of the maximum perturbation to the velocity occur within 10–20 m of the ground ($\sim \kappa u_* t / \ln(\kappa u_* t / z_0) \sim \ell_\theta / \ln(\ell_\theta / z_0)$), so that the numerical computations require high resolution to provide accurate prediction.
2. These distortions of the profiles increase with time (or distance) after the change in surface heating until $t \sim t_{MO}$. Then the perturbation analysis breaks down. But when $h/|L_{MO}| \gg 1$ the perturbation profiles can persist over very long periods (compared to the natural diffusion time in the boundary layer h/u_*). This is consistent with previous findings that strong stably/unstably stratified shear profiles (i.e. $|Ri| \gtrsim Ri_{crit}$ and $h/|L_{MO}| \gg 1$) do not necessary return to their basic state when perturbed. In fact they can develop into alternative persistent states (Galmiche and Hunt, 2002; Krishnamurti and Howard, 1981).
3. Previous studies have suggested that the formation of distorted profiles, including jets, is caused by the combined action of turbulence effects of stable stratification and Coriolis acceleration. However, our studies have shown that Coriolis effects are not essential for the development of jets, at least for the basic flow considered here. Indeed they tend to limit the perturbation rather than amplify them. But they have a significant effect on the fully developed or asymptotic states of the boundary layer. The Coriolis time-scale,

$1/f$, defines the maximum time over which changes in surface conditions must occur for unsteady profiles to be developed in the ABL, such as those studied here.

Acknowledgements

We are grateful for useful conversations with E. J. Hinch and A. S. Smedman and the referees helpful comments. This work was supported by financial support from the British Council and the German Academic Exchange Service (DAAD), the Deutsche Forschungsgemeinschaft (DFG) grant KL611/6-3 and grants from NERC to CPOM, UCL. JCRH is grateful to the Mechanical and Aerospace Engineering Department, Cornell University where he is the Mary B. Upson visiting Professor.

References

- Blackadar, A. K.: 1957, 'Boundary Layer Wind Maxima and Their Significance for the Growth of Nocturnal Inversions', *Bull. Amer. Meteor. Soc.*, **38**, 283-290.
- Bonner, W. D.: 1968, 'Climatology of the Low-Level Jet', *Mon. Weather Rev.*, **96**, 833-850.
- Businger, J. A., Wyngaard, J. C., Izumi, Y., Bradley, E. F.: 1971, 'Flux-Profile Relationships in the Atmospheric Surface Layer', *J. Atmos. Sci.*, **28**, 181-189.
- Clark, P. A. and Hopwood, W. P.: 2001, 'One-dimensional Site-Specific Forecasting of Radiation Fog. Part I: Model Formulation and Idealised Sensitivity Studies', *Meteorol. Appl.*, **8**, 279-286.
- Cullen, M. J. P.: 1993, 'The Unified Forecast/Climate Model', *Meteor. Mag.*, **122**, 81-94.
- Cullen, M. J. P., Davies, T. and Mawson, M. H.: 1993, 'Conservative Finite Difference Schemes for a Unified Forecast/Climate Model', *Unified Model documentation paper No. 10*, UK Met. Office, UK.
- Derbyshire, S. H.: 1994, 'A Balanced Approach to Stable Boundary Layer Dynamics', *J. Atmos. Sci.*, **51**, 3486-3504.
- Galmiche, M. and Hunt, J. C. R.: 2002, 'The Formation of Shear and Density Layers in Stably Stratified Turbulent Flows: Linear Processes', *J. Fluid Mech.*, **455**, 243-262.
- Garg, S. C., Maini, H. K., Thomas, J., Tiwari, M. K., Singh, V., Singh, D., Bahl, M., Khanna, R. M. and Gera, B. S.: 2004 'A New Temperature Inversion Layer Close to the Ground in Polluted Atmospheric Environment', *Proc. of the 12th Int. Sym. on Acoustic Remote Sensing*, Cambridge University, Cambridge, UK, July 11-16 63-66.
- Garratt, J. R.: 1992, *The Atmospheric Boundary Layer*, Cambridge University Press, Cambridge, UK, 316pp.
- Hinch, E. J. and Schubert, G.: 1971, 'Strong Streaming Induced by Moving Thermal Wave', *J. Fluid Mech.*, **47**, 291-304.

- Hunt, J. C. R., Stretch, D. D. and Britter, R. E.: 1988, 'Length Scales in Stably Stratified Turbulent Flows and Their Use in Turbulence Models,' In J.S. Puttock (ed.), *Proc. I.M.A. Conf. on Stably Stratified Flow and Dense Gas Dispersion*, Clarendon Press, Oxford, UK, 285–322.
- Hunt, J. C. R., Fernando, H. J. S. and Princevac, M.: 2003a, 'Unsteady Thermally Driven Flows on Gentle Slopes', *J. Atmos. Sci.*, **60**, 2169–2182.
- Hunt, J. C. R., Vrieling, A. J., Nieuwstadt F. T. N. and Fernando, H. J. S.: 2003b, 'The Influence of the Thermal Diffusivity of the Lower Boundary on Eddy Motion in Convection', *J. Fluid. Mech.*, **491**, 183–205.
- King, J. C. and Turner, J.: 1997, *Antarctic Meteorology and Climatology*, Cambridge University Press, Cambridge, UK, 425 pp.
- Krishnamurti, R. and Howard, L. N.: 1981, 'Large-Scale Flow Generation in Turbulent Convection'. *Proc. Natl. Acad. Sci. USA*, **78**, 1981-1985.
- Mulhearn, P. J.: 1981, 'On the Formation of a Stably Stratified Internal Boundary layer by Advection of Warmer Air Over a Cooler Sea', *Boundary-Layer Meteorol.*, **21**, 247–254.
- Monin, A. S. and Obukhov, A. M.: 1954, 'Basic Laws of Turbulent Mixing in the Ground Layer of Atmosphere', *Tr. Geofiz. Akad. Nauk. SSR.*, **1**, 95–115.
- Nieuwstadt, F. T. M. and Hunt, J. C. R.: 2003, 'Boundary Layers: Coherent Structures', In J. R. Holton (Editor-in-Chief), *Encyclopedia of Atmospheric Sciences*, Elsevier Science Ltd, London, UK, 228-233.
- Ooms, G. and Tennekes, H. (Eds.): 1984, *Atmospheric Dispersion of Heavy Gases and Small Particles*, IUTAM symposium, Delft, The Netherlands, August 29-September 2, 1983, Springer-Verlag, Berlin, Germany, 440pp.
- Rao, K. G. and Narasimha, R.: 1996, 'Estimation of Drag Coefficient at Low Wind Speeds Over the Monsoon Trough Land Region During MONTBLEX-90', *Geophys. Res. Lett.*, **23**, 2617–2620.
- Richardson, L. F.: 1923, 'Wind Above the Night-Calm at Benson at 7 a.m.', *Q. J. R. Meteorol. Soc.*, **49**, 34.
- Rider, N. E., Philip, J. R. and Bradley, E. F.: 1963, 'The Horizontal Transport of Heat and Moisture - A Micrometeorological Study', *Q. J. R. Meteorol. Soc.*, **89**, 507–531.
- Scorer, R. S.: 1954, 'Theory of Airflow over Mountains: IV – Separation of Flow over the Surface', *Q. J. R. Meteorol. Soc.*, **81**, 340–350.
- Simpson, J. E.: 1994, *Sea Breeze and Local Wind*, Cambridge University Press, Cambridge, UK, 234pp.
- Singal, S. P., Aggarwal, S. K., Pahwa, D. R. and Gera, B. S.: 1985, 'Stability Studies With the Help of Acoustic Sounding', *Atmospheric Environment*, **19**, 221-228.
- Smedman, A.-S., Bergström, H., and Högström, U.: 1995, 'Spectra, Variances and Length Scales in a Marine Boundary Layer Dominated by a Low Level Jet', *Boundary-Layer Meteorol.*, **76**, 211–232.
- Smedman, A. S., Högström, U. and Hunt, J. C. R.: 2004, 'Effects of Shear Sheltering in a Stable Atmospheric Boundary Layer with Strong Shear', *Q. J. R. Meteorol. Soc.*, **130**, 31–50.
- Thorpe, A. J. and Guymer, T. H.: 1977 'The Nocturnal Jet', *Q. J. R. Meteorol. Soc.*, **103**, 633–653.
- Townsend, A. A.: 1965, 'The Response of a Turbulent Boundary Layer to Abrupt Changes in Surface Conditions', *J. Fluid Mech.*, **22**, 799–822.
- Townsend, A. A.: 1976, *Structure of Turbulent Shear Flow*, Cambridge University Press, Cambridge, UK.

- Turner, J. S.: 1973, *Buoyancy Effects in Fluids*, Cambridge University Press, Cambridge, UK, 382pp.
- Wyngaard, J. C. and Brost, R. A.: 1984, 'Top-Down and Bottom-Up Diffusion of a Scalar in the Convective Boundary Layer', *J. Atmos. Sci.*, **41**, 102-112.

Address for Offprints: Antony Z. Owinoh, Potsdam Institute for Climate Impact Research (PIK), Telegrafenberg A31, D-14473 Potsdam, Germany.

